SURFACE PRESSURE AND SHEAR FORCE FIELDS MEASUREMENTS USING ELASTIC POLYMERIC FILM

Sergey D. Fonov, Larry P. Goss, Grant E. Jones, Jim W. Crafton, Vladimir S. Fonov
Innovative Scientific Solutions Inc, Dayton, OH
Michael Ol
Wright Patterson AFRL, Dayton, OH

Keywords: *shear stress, S3F, image processing*

ABSTRACT

The measurement principle behind Surface Stress Sensitive Films (S^3F) is based on the transformation of the measured deformation of an elastic media into surface loads (pressure and shear stresses). According to Gook's Law, the 3D deformation of the surface of an elastic film is a function of the applied tangential and normal tensions. Such displacements can be measured using several different 3D displacement techniques.

The results presented in the paper demonstrate that a stable S^3F can be created having a shift modulus between 30 - 50 Pa. Such highly sensitive elastic films provide the possibility of conducting surface stress field visualization with a resolution up to 0.1 Pa.

S^3F's are chemically inert and have small dielectric and optical losses. These features permit their use in liquid and various gaseous environments. Their properties are linear over a wide range of deformation (up to 10% - 15% of the film thickness) and can be adjusted by changing the chemical composition. This paper describes the measurement methodology and data-reduction algorithms currently used with the S^3F technique. Experimental results obtained with an S^3F optimized for low speed measurements, i.e., 5-50m/s (air flow) and 0.1-0.5m/s (water flow), are presented and analyzed. A comparative analysis of the S^3F and PSP techniques for a low speed air flow is presented..

1. BACKGROUND

Convenient, reliable and inexpensive methods for determining surface pressures, particularly of aerodynamic objects, have been the focus of many instrumentation developers. The standard approach with aerodynamic models is to use pressure taps, which are drilled into the surface under study and connected via tubing to multiplexed pressure gages or pressure gage arrays. Hundreds of pressure taps are required to get the complete pressure distribution on a model's surface. However, this is typically impractical, so sophisticated interpolation procedures are employed to generate the distribution between distant taps [1]. Pressure taps provide information only about the static or normal pressure components acting on the surface. Tangential pressure components or shear stresses should also be measured. In the past shear stress components were measured indirectly by either heat flux measurements, by miniature balance systems imbedded into model surface, or by measuring the shear force acting on a floating element located on the model's surface [2,3].

In 1980, Peterson and Fitzgerald proposed using oxygen quenching of fluorescent dyes for flow visualization [4]. A similar approach was patented by Pervushin and Nevsky [5]. Since this early work, much effort has gone into the development of the Pressure Sensitive Paint (PSP) measurement technique [6]. PSP is based on oxygen quenching of molecular photoluminescence. In practice, a surface under study is covered by thin a polymer layer which is embedded with

luminophore molecules. Oxygen from the ambient flow can diffuse within the polymeric layer were its concentration is proportional to the static air pressure at the surface. An appropriate light source is used to excite the luminescence molecules. The total luminescence output from the layer is a function of the local oxygen concentration due to oxygen quenching [7].

The oxygen diffusion in the PSP layer determines the layer's response time to a pressure change on the surface [8]. This response time can be estimated as $\tau \approx \Lambda^2 / D$, where Λ is the PSP layer thickness and D – is the oxygen diffusion coefficient. For practically layer thicknesses of 1-2 μm, the response time is ~ 2 - 4 ms which represents an upper limit for using PSP to investigate transient phenomena in air flows.

The normalized luminescence output function I/Io of PSPs can be approximated by (see Fig. 1):

$$I/Io=1/[(A(T)+B(T)P] \tag{1}$$

where Io – is the output at P=0.0, A(T) and B(T) are functions of the local layer temperature T, and P is the static pressure.
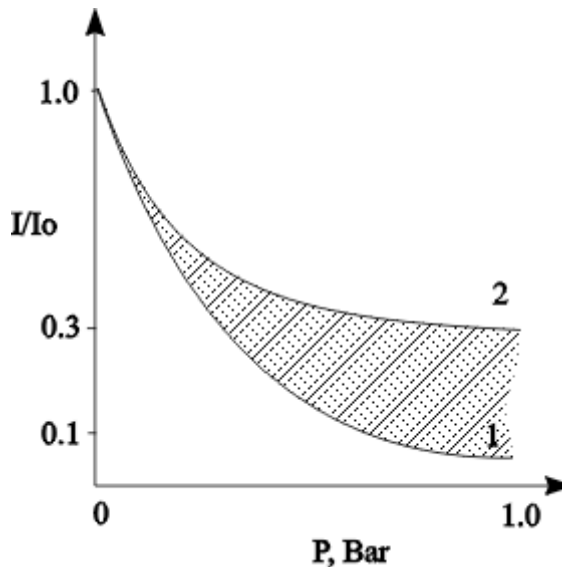
Fig. 1 - Relative intensity as function of pressure for Pressure Sensitive Paints.

PSP based on oxygen quenching is essentially an absolute pressure gage, and all workable formulations can be located between curve 1 and 2 of Fig. 1. PSP sensitivity dI/dP is a function of the pressure level and dramatically decreases as $1/P^2$ which causes problems for low speed flows. The pressure dependence can be linearized using the Stern-Former approximation:

$$Ir(P,T)=Io/I = A(T)+B(T)*P \tag{2}$$

The sensitivity dIr/dP for most currently available PSP formulations vary in the range between $(0.5 -1.0)*10^{-3}$%/Pa and can not be significantly increased. As noted above, this represents a major problem for appling PSP to low-speed flows. Take for example low subsonic velocities where the Mach number is below 0.05. The pressure variation on the model is proportional to the square of the Mach number. The pressure range δP for Ma=0.05 (V=35mile/h) is about 100Pa which is hundred time less than at M=0.5 (V=350mile/h and $\delta P=10^4$Pa). However, the PSP

sensitivity can't be modified to match the low speed requirement. The only approach to getting reliable results at low speeds is to increase the signal to noise ratio in the acquired data and to minimize all error sources, i.e., illumination non-stability, model displacement and deformation, and temperature effects. The temperature sensitivity of PSPs varies between 100Pa/^{o}C to 1000Pa/^{o}C which is comparable with the total pressure variation expected for Ma=0.05. Most PSP measurements at flow velocities (below Ma=0.05) are typically semi-quantitative and require significant experimental efforts.

Mapping of the shear stresses has been accomplished to date on a semi-quantitative level using either liquid crystals [9] or oil films [10]. In the early nineties methods for direct measurement of surface shear force began to appear in the literature [11, 12]. One such method included mounting on the model surface a sensing element in the form of a film made of a flexible polymeric gel having a small thickness with a low shear module. Shear deformation of the film caused by the flow is measured by monitoring the displacement of markers applied to the film. The shearing stress is determined by using Hooke's law for shear strain. The film markers could be made in the form of a reflection grating placed on the model's surface(under the film) and a transmitting grating on the film's surface enabling the use of the moiré technique for recording shear strain. This method provided improved accuracy and informative capacity due to determining local values of the shearing stress. The main drawback of this method is that gradients of the normal pressure also create shear displacement of polymer gel, thus, this method works best in the absence of normal pressure gradients.

To understand why this is a problem let's consider a model 2-D case of a vortex interaction with an elastic polymer surface presented in Fig. 2. The vortex is characterized by circulation Γ, is located at distance h from an elastic surface, and is placed in the bottom of a cavity. The elastic polymer has thickness H and shear module G. Results of an FEA solution of the joint Navier-Stokes equations and Lame system of elasticity are presented at Figs. 3 and 4. The velocity and pressure fields near by the elastic polymer are plotted in Fig. 4 (air ,Re=1000 h=2mm). Figure 5 displays plots of the pressure and friction force distributions and results of their action on the elastic polymer – normal and tangential deformation for G=600Pa and H=1mm. The vortex-surface interaction creates a large local variation in the flow velocity accompanied by a local gradient in the pressure and friction forces. The magnitude of the friction force is smaller than the pressure force and the resulting surface deformations are mainly due to pressure. The adequate treatment of these deformations fields requires development of a data processing scheme which takes into account both the pressure and friction fields.

2.   NEW APPROACH

The main goal of the present work was to provide a method for measuring the static pressure of fluids on a surface, which does not suffer from the drawbacks of PSPs based on oxygen-quenching, i.e., the necessity for oxygen in the fluid, the need for a compressible fluid, and a limited pressure sensitivity and frequency response.

A secondary goal was to provide a method for measuring the shear stress of fluids on a surface, which can work in the presence of normal pressures and provides a means to resolve normal and shear tension components. Both goals also must be supported by a means for direct calibration.
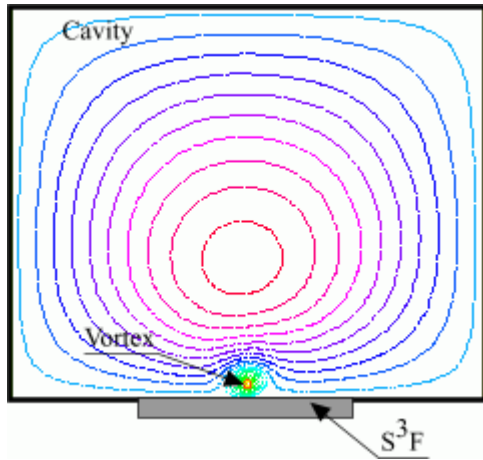
Fig. 2 - Vortex in a cavity.
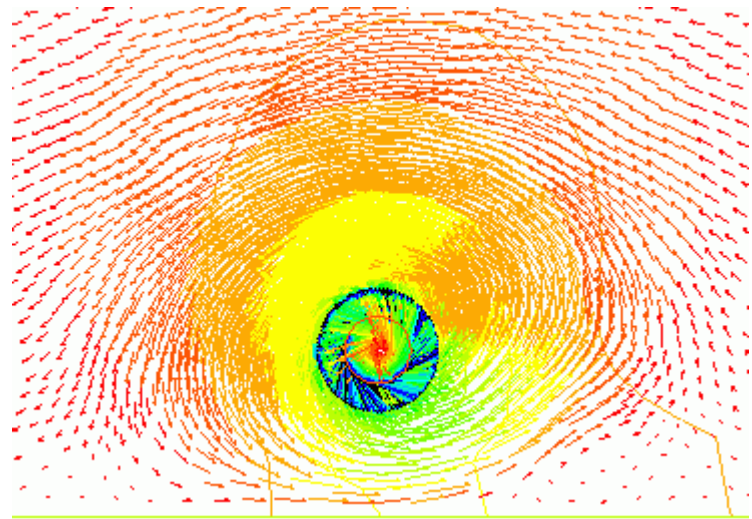
Fig. 3 - Velocity and pressure fields near by elastic polymer surface generated by vortex (Re=1000, h=2mm, $\Gamma=2\pi*0.5mm*15m/s$, air).
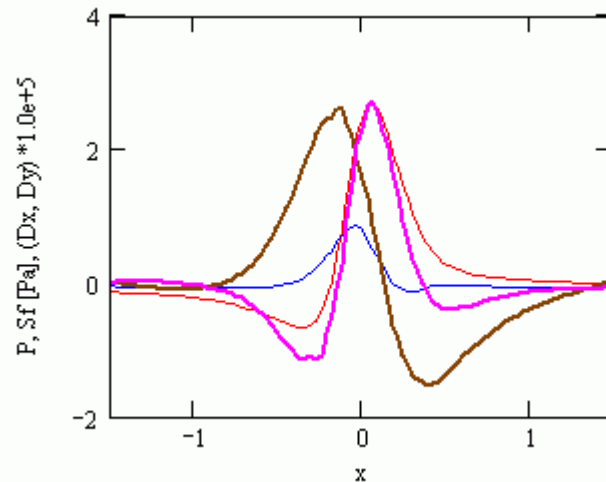
Fig. 4 - Pressure (red), friction (blue) stresses, normal (magenta) and tangential (brown) deformations.

The standard approach for obtaining high measurement accuracy is to increase the gage's sensitivity by measuring increments relative to some etalon value located in the measurement range, i.e., using for example a differential pressure gage instead of an absolute pressure gage. This idea of a differential pressure measurement is the cornerstone of the S^3F technique. The elastic polymer behaves like a non-compressible fluid but contrary to most fluids it tries to recover its original shape after removal of the deformation force.

Pressure loads P1 and P2 applied to a surface (see Fig. 5) will displace the elastic material resulting in a change in the local layer thickness of $\delta\Lambda \sim Cp(P2-P1)$. This is only a crude representation, because in general the deformations of the elastic polymer layer are also governed by pressure gradients and shear force.
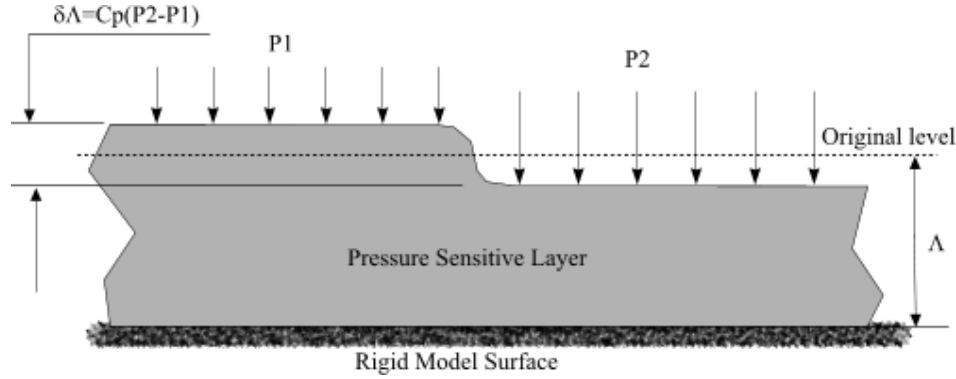
Fig. 5 - Realization of the differential principle.

The linear frequency response of the elastic film is limited by the natural frequency of the shear oscillation and can be estimated as

$$f_0 = 2\pi \sqrt{\frac{G}{\rho h^2}}$$

Tuning $G \in (100\dots1000)$Pa, and $h \in (0.1..1)$mm, it is possible to adjust the film's frequency response in the range of 2-60KHz which is ~ 100 times better than that of standard PSPs based on oxygen quenching.

In order for a elastic polymer to produce the desired results it must be applied to the surface under study. There are several ways to apply these films including airbrush spraying and "shrink-fit method". The latter approach provides a film with a controlled thickness and was used for this evaluation. Source components are poured into a flat cavity having a smoothed bottom. After polymerization, the film is pealed off and placed on the model under study. The film thickness can be estimated by direct measurements using for example optical absorption or a capacitor type thickness gage. The next step is the film calibration. The calibration procedure includes the application of a specific load onto the film surface and measuring the corresponding normal deformation which allows evaluation of the film response function. The smaller the load area, the more the film response function will correspond to an impulse function.

Consider for simplicity a 1D applied load. In this case, the deformation can be treated in 2D space. Assume a cavity with a rectangular cross-section [0,20]x[0,1]. The cavity is filled with an elastic polymer (S³F) with a characteristic thickness (d=1 mm). Concentrated constant loads (normal or tangential) are applied at the interval [9.9, 10.1]. Zero deformations on the cavity walls determine the boundary conditions for this problem.

The S³F is an elastic solid and is deformed under the applied forces. A point in the solid, originally at (x,y) goes to (X,Y) upon application of the load. If the displacement vector $\vec{r} = (r_1, r_2) = (X - x, Y - y)$ is small, Hooke's law relates the stress tensor σ inside the solids to the deformation tensor ε [13]:

$$\sigma_{ij} = \lambda \delta_{ij} \nabla \cdot \vec{r} + \mu \varepsilon_{ij}, \quad \varepsilon_{ij} = \frac{1}{2}\left(\frac{\partial r_i}{\partial x_j} + \frac{\partial r_j}{\partial x_i} \right) \qquad (3)$$

Here δ is the Kronecker symbol and λ, μ are two constants describing the material mechanical properties in terms of the modulus of elasticity, and the Young's modulus.

The equation of elasticity is written in a variant form for the displacement vector $\vec{r}(x) \in \Omega$ as

$$\int_{\Omega} \left[\mu \varepsilon_{ij}(\vec{r}) \varepsilon_{ij}(\vec{w}) + \lambda \varepsilon_{ii}(\vec{r}) \varepsilon_{jj}(\vec{w}) \right] = \int_{\Gamma} \vec{\tau} \cdot \vec{w}, \quad \forall \vec{w} \in \Omega \qquad (4)$$

where Γ - is the cavity boundary and the integrals are written in the notations from reference 14. Solutions for a normal load are presented in Fig. 6. The displacement map (A) shows that the deformation is concentrated mainly in a region with a diameter about 2-3 times the thickness of the elastic layer (yellow zone). Both the deformed FE grid (B, zoomed) and displacement vector map (C, zoomed) confirm this result.
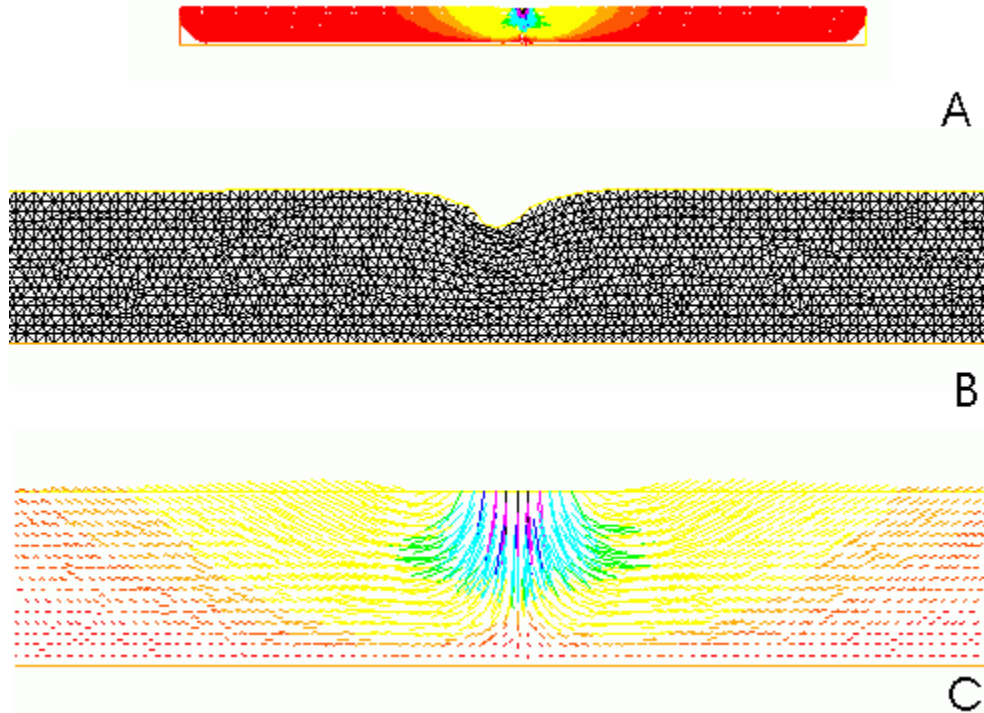
Fig. 6 - Solution of the normal surface load problem. (A- Relative geometry of the polymer layer with displacement map, B-zoomed view of the deformed FE grid, and C- displacement vector map).

Figure 7 displays the normal (blue line) and tangential (red line) displacements that result from the action of the applied rectangular pulse load (pink line) for the elastic polymer layer. Note that the magnitude of the tangential displacement is approximately two times larger than magnitude of the normal displacement in the region outside of the applied load. Thus, information about tangential displacement can also be used for normal force visualization. Of course the normal displacements below the region of the applied load are significantly larger. The normal displacement distribution $g(x)$ can be treated as the reaction of the elastomer to the pulse load $\delta(x)$. Assuming that the elastic reaction R(x) to the arbitrary load $L(x)$ can be treated as a linear system:

$$R(x) = \int g(x - x') L(x') dx' \qquad (5)$$
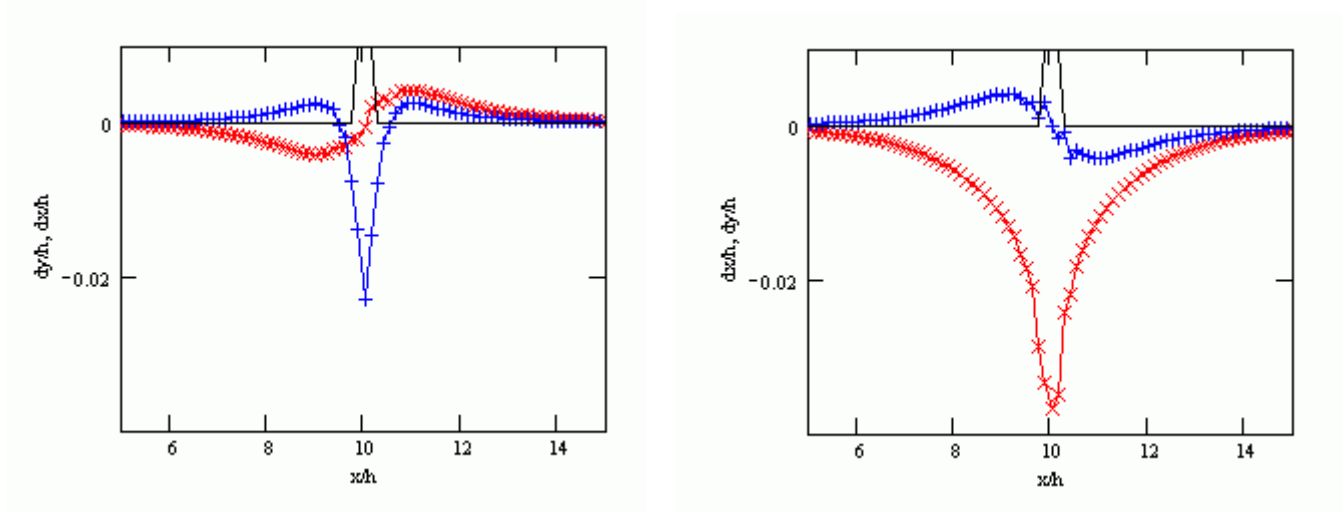
Fig. 7 - Displacements on the upper boundary, right plot -normal load, left plot – shear load 10 Pa, layer thickness h=1mm, E=600, v=0.495, (tangential displacement– red line, normal displacement – blue line, load distribution – black line).

The reaction due to the load $L_j =(L_{nj}, L_{sj})$ applied at the interval $[x_0, x_N]$ can be presented by:

$$R_{nj} = \sum_{k=0}^{N} L_{nk}\tilde{n}_n(x_j - x_k) + L_{gk}\tilde{s}_n(x_j - x_k) \qquad (6)$$

$$R_{sj} = \sum_{k=0}^{N} L_{nk}\tilde{n}_s(x_j - x_k) + L_{gk}\tilde{s}_s(x_j - x_k)$$

This system of linear equations (Eq. 6) with unknown L_k, has the diagonally dominant matrix (see Fig. 8) $G_{jk} = \begin{pmatrix} \tilde{n}_{njk} & \tilde{s}_{njk} \\ \tilde{n}_{sjk} & \tilde{s}_{sjk} \end{pmatrix}$, which can be inverted to yield the solution of linear equations:

$$L = G^{-1} \cdot R \qquad (7)$$
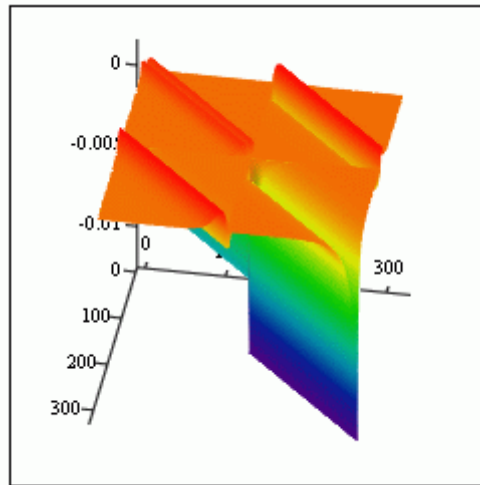
Fig. 8 - 3D presentation of G matrix.

7

To visualize the effectiveness of such an approach let's consider the reconstruction of a cosine type load. This case is presented in Fig. 9. A normal load distribution of $L(x) = (1 + \cos(2\pi(x-10)/D) \quad x \in [10 - D/2; 10 + D/2], \quad D = 5.0$ was used as input for FEA. The resulting normal displacement were used in Eq. 5 with the matrix G^{-1} taken from the estimation of the pulse load.
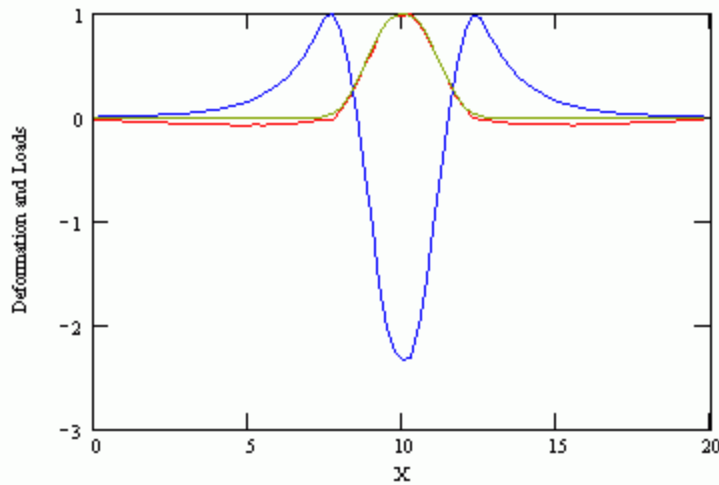
Fig. 9 - "Cosine" Load (brown curve) creates normal displacement (blue curve) which is transformed in load distribution (red curve).

The average error between the applied and recovered load is less then 1% on the applied load interval and grows up to 3% outside this interval. This result indicates that smooth loads can be recovered with acceptable accuracy by employing a simple model.

The response of the film to a load depends on the film thickness. Figure 10 presents FEA modeling results of the film's response function due to a rectangular load as a function of relative film thickness. Figures 10 emphasizes that the film thickness distribution must be taken into account for gage calibration.

Shear displacements can be measured by applying markers to the surface of the film and recording their displacement due to applied loads. Additional marker patterns applied to the substrate can be used for image registering before ratioing, thus, compensating for model movement and deformation under aerodynamic or inertia forces. A cross-correlation analysis applied to the load-off and load-on image pairs provides the 2D shear displacement field.

3. EXPERIMENTAL EXAMPLES

The Shear Stress Module is the main parameter that determines the sensitivity of S^3F. This parameter can be measured directly by applying shear force to the film and measuring the corresponding displacement. It is possible to create a stable S^3F having a shear stress module in the range of G= 30-3000 Pa.
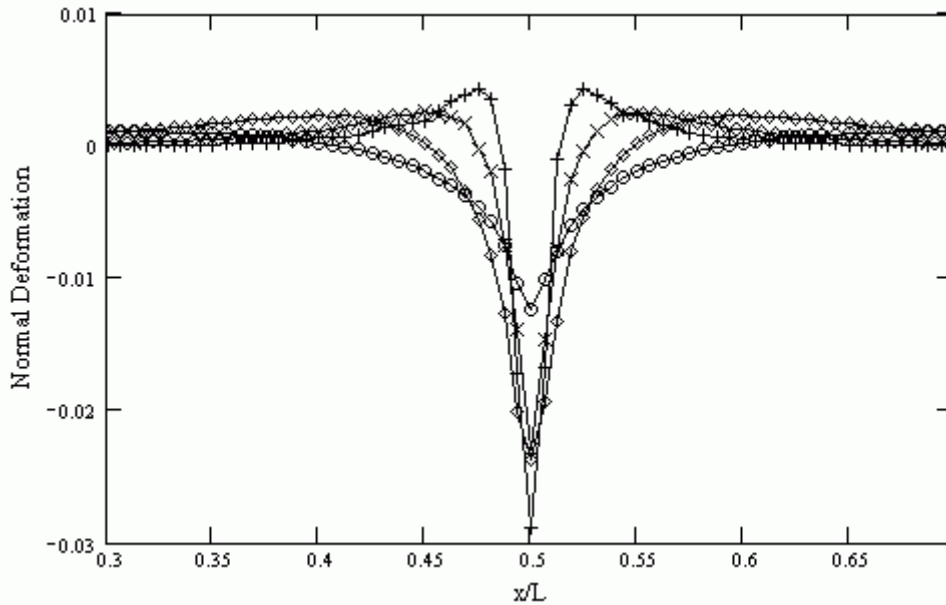
Fig. 10 - Normal responses on normal rectangular load for relative film thicknesses ("x" – 1, "o" -4, "+" -0.5, "◊" -2).

Figure 11 depicts the calibration of an S^3F. This composition displays good linearity and a small hysteresis, which is in the range of the tangential displacement measurement accuracy σ=0.1-0.3µm. The total linear dynamic range of the displacement is ~ 1000 µm which is relatively large compared with the S^3F layer thickness in this case of 1730 µm.
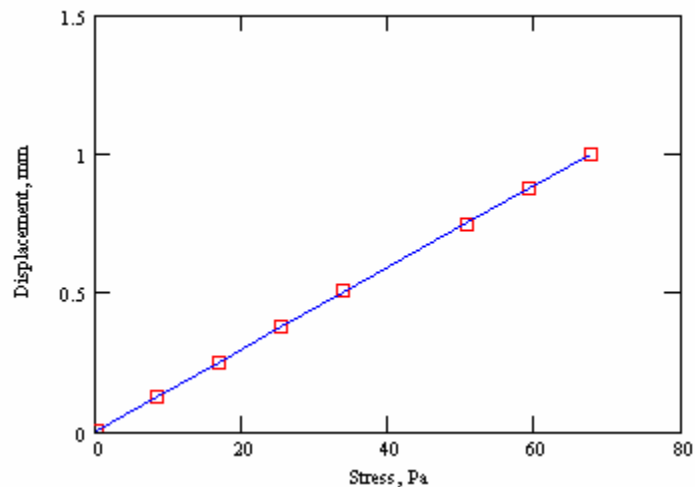
Fig. 11 - Calibration curve for S^3F composition with shear stress module 117Pa.

The experimental setup for S^3F measurements is shown in Fig. 12. All three deformation components (D_x, H, D_z) are extracted from the wind-off and wind-on images taken by the high-resolution CCD camera.

The first attempt to use the S^3F technique for pressure field visualization showed very promising results. Successful visualizations have been conducted for flow velocities varing from 0.1 m/s to 1m/s (in water), and from 10m/s to 45m/s in air flow. S^3F is sensitive to both the
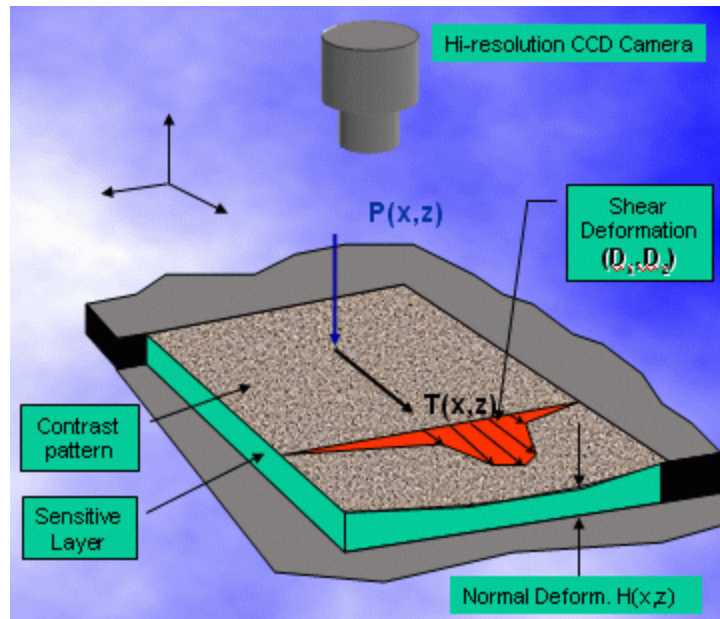
Fig. 12 - Typical measurement schematic for S³F applications.

normal and tangential (shear) forces applied to the surface as well as to the inertial forces applied to the volume.

A delta wing model was tested at a flow velocity of 15 m/s and an angle of attack 10°. The surface was covered with S³F having a thickness of 1 mm. A fine low density powder was applied to the surface of the S³F to create a pattern for the shear deformation measurements. The relative thickness distribution for the S³F is shown in Fig. 13a. The vortex above the wing surface creates a narrow decompression region with a pressure gradient oriented mainly across the ambient flow direction. Thus, each cross section of the elastic deformation can be treated as plane. A cross-correlation analysis provided the shear displacement field results presented in Fig. 13b. The vertical component of the shear displacement vector presented in false color yields information about the local shear force distribution under the vortex flow.

The pressure recovery results based on the above described data treatment procedure are presented in Figs. 14 and 15.

The pressure field shown in Fig. 16 was obtained using a PSP under the identical flow conditions. To obtain a PSP pressure field with the same SNR it was necessary to acquire and average 64 images for both the wind-off and wind-on conditions and to apply adaptive filtering with a window 25 by 5 pixel on the resected images. The S³F sensitivity was about 25 times higher and a comparable SNR was obtained by acquiring only 1 wind-off and wind-on image.
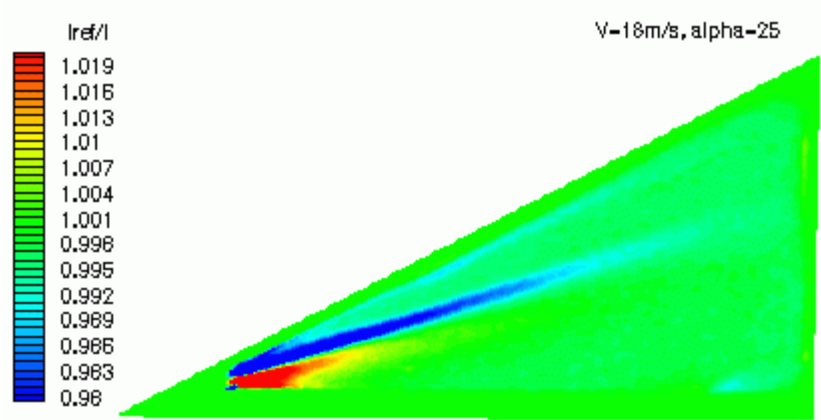
Fig. 13a - Relative thickness distribution on the surface of the delta wing model. Flow velocity 18m/s, angle of attack 12°.
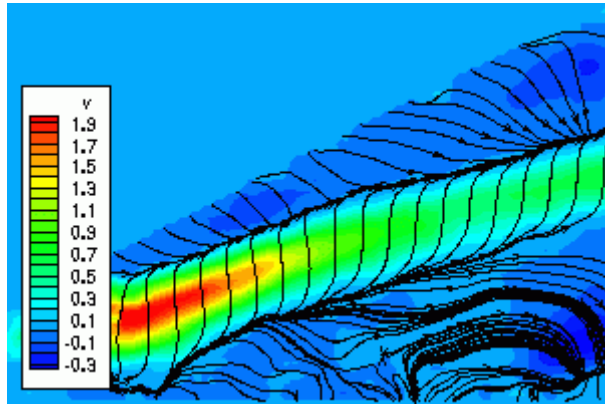
Fig. 13b - Shear vector field and vertical component of shear vector (expressed in pixels - false color presentation) on the surface of the delta wing model. V=18m/s, α=12°
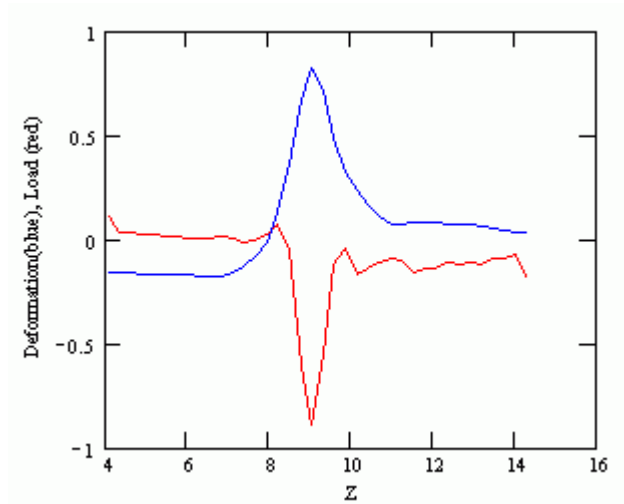
Fig. 14 - Relative displacement (blue) and reconstructed pressure distribution (red) for section x=0.3.
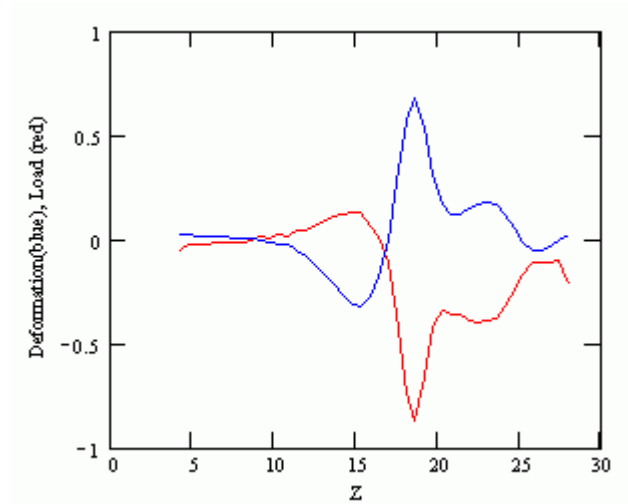
Fig. 15 - Relative displacement (blue) and reconstructed pressure distribution (red) for section x=0.5.
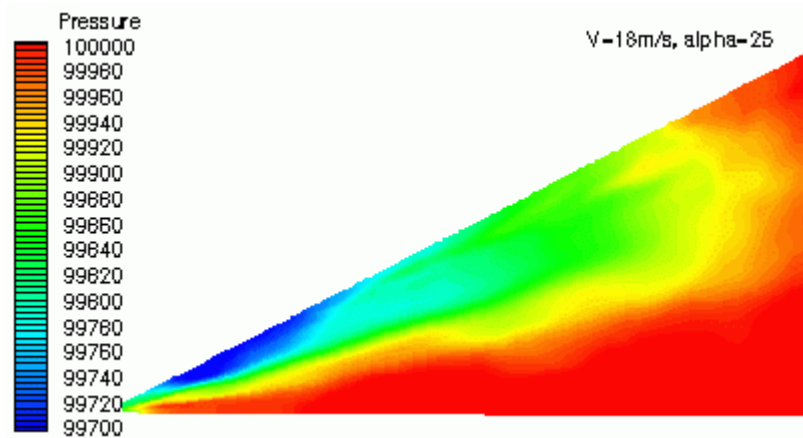
Fig. 16 - Pressure field , PSP results, V=18m/s, α=12°.

Pressure distribution measurements on models immersed in water are an attractive application for S[3]F since standard PSPs do not work well in water due to low oxygen levels and very low compressibility. Measurements with S[3]F have been conducted in the WPAFB-AFRT water tunnel. The first model to be tested was a double delta wing shown in Fig. 17. S[3]F was created in a cavity having a thickness H=1.5mm and shear module in the range 30 – 60Pa. These film properties in combination with the spatial resolution of the 3D deformation measurements (1 μm), provided for a pressure and shear force measurement resolution of ~ 0.1- 0.2 Pa.

Figure 18 shows the streamlines of the shear and normal (false color) components of the 3D deformation field. All deformations are normalized to the S[3]F thickness, H. The influence of the vortex flow on the shear deformation field is clearly visualized. The deformation field is significantly three-dimensional in this case, and only at the beginning of the vortex (near by section A-A) can the 2D approach for load reconstruction (discussed earlier) be applied. Figure 19 displays components of the deformation field in section A-A (coordinate system is tilted around Z-axis in the direction of vortex axis.

The recovered normal and shear stress component for section A-A are presented in Fig. 20. An additional adaptive filtering procedure was applied to smooth the reconstructed data (points).

4.   CONCLUSIONS

The S[3]F technique demonstrates the ability to conduct quantitative pressure and friction force visualization with a resolution up to 0.05-0.2Pa in any optically transparent fluid. The data processing scheme for S[3]F is more complex than for PSP and requires further development and investigation.
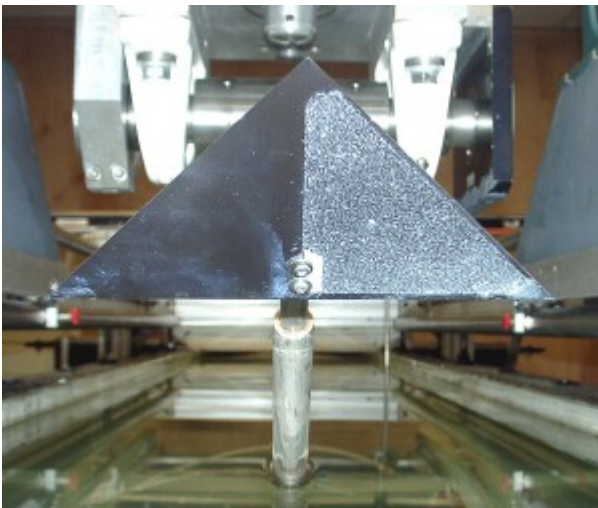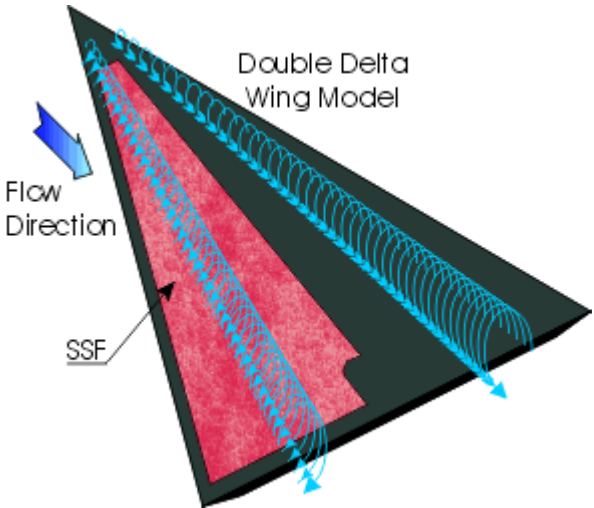
Fig. 17 - Double Delta Wing Model with S3F (pink color on left image)
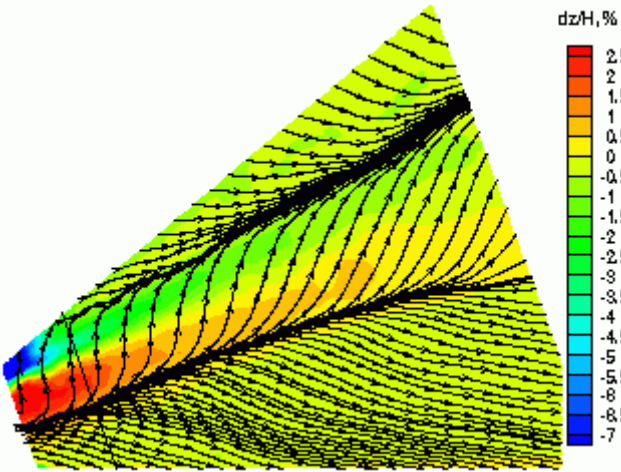
Fig. 18 - Visualization of the tangential (streamlines) and normal (false color) deformation fields on the Delta Wing Model (angle of attack 15°, water flow velocity 0.4 m/s)
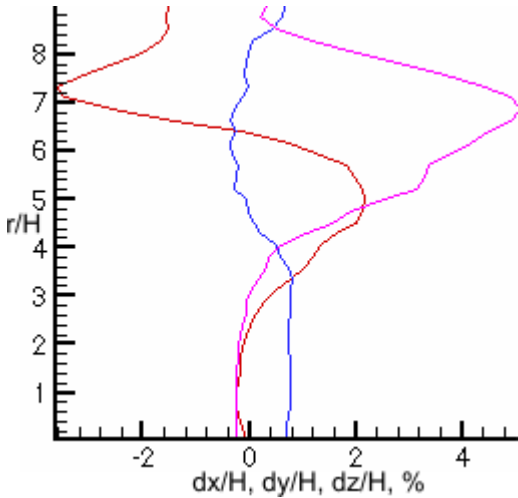
Fig. 19- Deformation components in the section A-A (dx/H - blue, dy/H -pink and dz/H – brown lines)
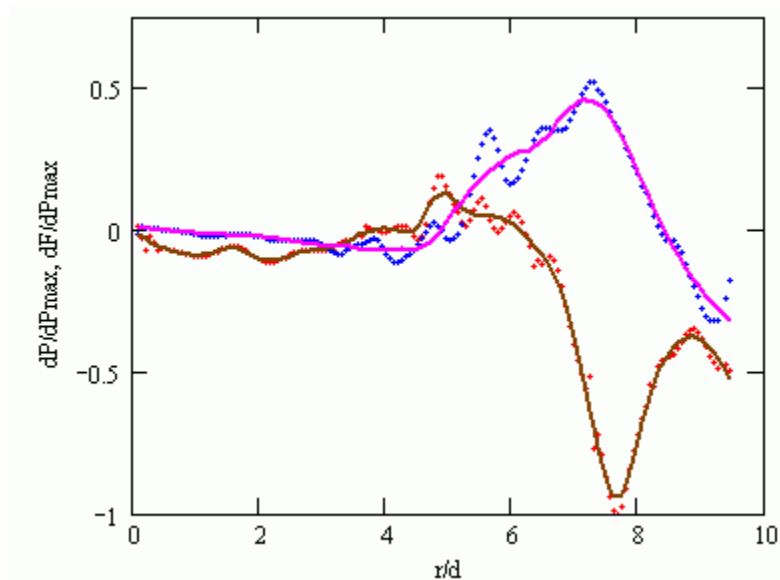
Fig. 20 - Normal (brown) and shear (pink) stress components for section A-A.

REFERENCES

1. Jewel B. Barlow, William H. Rae, Alan Pope, "Low-Speed Wind Tunnel Testing", Wiley, John & Sons, Inc., 1999, 800pp.
2. Magill et al., "Study of a Direct Measuring Skin Friction Gage with Rubber Compounds for Damping", AIAA Paper 2000-2395).
3. J.W. Naughton, M. Sheplak "Modern Development in Shear Stress Measurement", Progress in Aerospace Sciences 38(2002) 515-570
4. Peterson, J.I. et al., "New Technique of Surface Flow Visualization Based on Oxygen Quenching of Fluorescence", Rev. Sci. Instrum. 51(5):670-671, 1980
5. Nevsky, L.B.; Pervushin, G.E. "Method of pressure distribution measurement with the indicating coating" Patent SU 1065452/1981
6. Bell James H et al. "Surface Pressure Measurements Using Luminescence Coatings" Annual Rev. Fluid Mech. 2001. 33:155-206.
7. Mosharov V, Radchenko V, Fonov S. "Luminescent Pressure Sensors in Aerodynamic Experiment", Moscow: TsAGI, CWA Int. Corp. 1997
8. Fonov S., Mosharov V., Radchenko V., Mihailov S. Kulesh V.   "Application of the PSP for investigation of the oscillating pressure fields" AIAA Paper 98-2503, Presented at Appl. Aerodyn. Conf., 16th, Albuquerque, NM 1998.
9. Reda D.V. "Measurements of continuous pressure and shear distributions using coating and imaging techniques", AIAA Journal v.36, pp. 895-899, 1998.
10. Zhong, S. "Detection of flow separation and reattachment using shear-sensitive liquid crystals", Experiment in Fluids, v.32 pp.667-673, 2002
11. Tarasov V.N, Orlov A.A. "Method for determining shear stress on aerodynamic model surface", Patent of Russia, 4841553/23/1990
12. Tarasov V., S. Fonov, A. Morozov, "New gauges for direct skin friction measurements." Proc. Of 17th International Congress on Instrumentation in Aerospace Simulation Facilities (ICIASF), Monterey, California, 29 Sept to 2 Oct 1997.
13. Landau L.D, Lifshitz E.M. "Course of Theoretical Physics: Theory of Elasticity", Vol. 7 Butterworth-Heinemann, 1995, 260pp
14. Braess D. "Finite Element", Second Edition, Cambridge University Press, 2001